One-step photoemission calculations for ideal GaAs(001) and AlAs(001) surfaces and $(GaAs)_m(AlAs)_n$ superlattices

T. Strasser, C. Solterbeck, and W. Schattke
Institut für Theoretische Physik und Astrophysik, Christian-Albrechts-Universität, Leibnizstrasse 15, D-24098 Kiel, Germany

I. Bartoš, M. Cukr, and P. Jiříček
Institute of Physics, Academy of Sciences of the Czech Republic, Cukrovarnická 10, 16253 Prague 6, Czech Republic

C. S. Fadley and M. A. Van Hove
Materials Sciences Division, Lawrence Berkeley National Laboratory, Berkeley, California 94720
Department of Physics, University of California, Davis, California 95616
(Received 18 November 2000; published 30 April 2001)

Normal photoemission spectra for the (001) surface of $(AlAs)_2(GaAs)_2$ and $(AlAs)_3(GaAs)_3$ superlattices are calculated. They represent the first calculations within the one-step model for layered superlattices. The aim is to develop tools to extract general features from measured spectra specific to superlattices. The spectra show the opening of band gaps at the Brillouin zone edge, which are characteristic for the modified periodicity of the superlattice. Furthermore, the layer-resolved photocurrent allows to identify emissions from AlAs layers hidden below the first two or three GaAs layers. As a reference, theoretical normal emission spectra from the pure bulk GaAs and AlAs(001) surfaces are shown.

DOI: 10.1103/PhysRevB.63.195321 PACS number(s): 73.20.At, 73.61.Ey, 71.20.Nr, 79.60.Jv

I. INTRODUCTION

Superlattices, formed by ultrathin layers of different semiconductor materials, are widely recognized for their unique electronic and optical properties.[1–3] These superlattices cannot be treated as being composed of layers with their individual band structures. On the contrary, the electronic properties are determined by the superlattice as a whole. The larger periodicity perpendicular to the surface changes the dimension of the Brillouin zone. This results in the back folding of the valence bands of the bulk material, accompanied by additional gaps at the edges of the Brillouin zone. Similar effects, due to surface reconstruction that increases the translation period and accordingly decreases the dimension of the surface Brillouin zone along the surface, have been reported recently from the point of view of photoemission.[4].

The nearly equal lattice constants of GaAs and AlAs together with the experimental possibility of molecular-beam epitaxy single out this system for a detailed analysis. Photoemission spectroscopy is widely used to examine the electronic structures of materials. The spectra give insight into the valence-band structure of the bulk as well as of the surface. Beside the initial states, photoemission involves the excitation to outgoing scattering states. In addition, the bulk features are superposed by surface emission and a full account of experimental data can only be attained by a comparison with photocurrents calculated within the one-step model of photoemission theory.

In this paper, we present one-step photoemission calculation for the (001) surface of GaAs/AlAs superlattices. Substantial attention is paid to the question how the periodicity of the superlattice influences the bulk electronic structure and what can be seen in the photocurrent. As a reference, results for GaAs and AlAs bulk crystals are given first. Afterwards, we discuss the photocurrent for $(AlAs)_2(GaAs)_2$ and $(AlAs)_3(GaAs)_3$ superlattices.

II. THEORY

The photocurrent is calculated within the one-step model. For details see Refs. 5,6. In this ''Golden rule'' formulation of the photoemission process, the photocurrent I at the photon energy $h\nu$ is given by

$$I \sim \sum_{i,j} \langle \Phi^*_{LEED}(E_{fin},k_\parallel)|\mathbf{A_0}\cdot\mathbf{p}|\Psi_i\rangle G_{i,j}(E_{fin}-h\nu,k_\parallel) \times \langle \Psi_j|\mathbf{p}\cdot\mathbf{A_0}|\Phi^*_{LEED}(E_{fin},k_\parallel)\rangle.$$

The vector potential $\mathbf{A}_0$ is kept constant, $\mathbf{p}$ denotes the momentum operator and $k_\parallel$ is the parallel momentum. The initial states are represented by a half-space Green's function. This Green's function $G_{i,j}$ is given in a layer resolved linear combination of atomic orbitals Ψ_i. Our basis set consists of the $4s$ and $4p$ atomic orbitals of gallium and arsenic and the $3s$ and $3p$ atomic orbitals of aluminum.[7] The associated Hamilton matrix is calculated according to the Extended-Hückel-Theory.[8–10] In this theory, a small number of parameters is used to determine the hamilton matrix $\hat{H}(\vec{k})$ in a basis of atomic orbitals from the matrix of orbital overlaps $S(\vec{k})$ as a function of Bloch vector $\vec{k}$. The following ansatz is used:

$$H_{\alpha l \alpha l} = -\tilde{I}_{\alpha l} - K_{\alpha\alpha} I_{\alpha l}[S_{\alpha l \alpha l}(\vec{k}) - 1],$$

$$H_{\beta m \alpha l} = -\frac{1}{2} K_{\alpha\beta}(I_{\alpha l} + I_{\beta m}) S_{\beta m \alpha l}(\vec{k}) \quad \text{for } (\alpha l) \neq (\beta m).$$

 ©2001 The American Physical Society

TABLE I. EHT parameter for GaAs and AlAs [for the notation see Starrost *et al.* (Ref. 10)].

Atom	K_{ss}	K_{sp}	K_{pp}	I_s	I_p	$\tilde{I}_s$	$\tilde{I}_p$
As (GaAs)	1.000	0.844	0.844	39.38	22.50	16.46	8.53
Ga (GaAs)	1.000	0.844	0.844	24.38	22.50	15.24	8.53
As (AlAs)	1.000	0.750	0.563	20.63	28.13	9.42	8.81
Al (AlAs)	1.000	0.750	0.563	30.00	39.38	19.17	10.03

Here α and β are the orbital symmetry labels and l and m are the indices for the basis atom in the unit cell. The parameters $\tilde{I}_{\alpha l}$ can be treated as the energy of the orbital α at atom l, $I_{\alpha l}$ introduce a species-dependent transfer energy. The parameters for GaAs and AlAs are listed in Ref. 10. Because they should be used to describe a heterostructure, we slightly modify the parameters $\tilde{I}_{\alpha l}$. They are adjusted to the valence-band offset between GaAs and AlAs of 0.45 eV.[11] The parameters as finally used are given in Table I. Figure 1 shows the resulting band structures for bulk GaAs and AlAs, together with the bands resulting from the original parameters. While in the case of GaAs, only the bulk bands (1,2) are notably affected by the modified $\tilde{I}_{\alpha l}$ parameters, for AlAs, the band widths change about 277 and 458 meV for the band (1,2) and (3) respectively. To get an agreement with the existing linear muffin-tin orbital (LMTO) calculation[12] it was necessary to modify also K parameters describing the connection between atoms in different GaAs and AlAs layers. For these atoms, the K parameters have been averaged between those from bulk GaAs and AlAs.

The electronic structure of the surface is determined by the calculation of the $k_{\parallel}$-resolved density of states (DOS) from the half-space Green's matrix $G_{i,j}$, the same as used for the photocurrent. The Green's matrix takes into account relaxation and reconstruction at the surface.

The final state of photoemission is a time-reversed low-energy electron diffraction (LEED)-state Φ^*_{LEED} with final-state energy E_{fin}. Its wave function is determined by matching the solution of the complex band structure to the vacuum solution, representing the surface by a step potential. The step position is fixed according to previous calculations for GaAs (Ref. 13) and for a better comparison kept constant for all calculations in this paper. The solution within the bulk is calculated by the empirical pseudopotential method, as described by Mäder and Zunger.[14] They developed a method that permits specifying the form factors for continuous reciprocal lattice vectors and tested them for GaAs and AlAs. The damping of the final state wave function inside the crystal is described by the imaginary part of an optical potential.

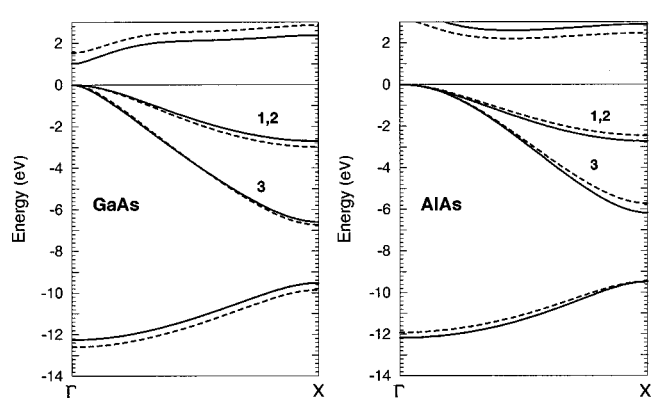

FIG. 1. The bulk band structures of GaAs and AlAs. Dotted lines: using the EHT parameters of Starrost *et al.* (Ref. 10). Solid lines: using the modified EHT parameters used for the superlattices (for details see text).

III. RESULTS AND DISCUSSION

A. GaAs(001)-(1×1)Ga

In this section, results for the ideal GaAs(001)-(1×1)Ga surface, i.e., Ga-terminated bulk structure, are presented. The main purpose is it to give a reference for the examination of the superlattices. The surface geometry is shown as an insert in Fig. 2, where also the surface Brillouin zone with some high-symmetry points is sketched. The same surface geometry is used also for the superlattices. Because the lattice constants of GaAs and AlAs are very similar, we used the lattice constant of GaAs for all calculations.

The surface band structure for the GaAs(001)−(1×1)Ga is shown in Fig. 2 together with the projected bulk band structure, which is shaded in gray. In the fundamental gap, there are two surface bands (a) and (b) which can be identified as a bridge and a dangling bond state respectively. The first one consists of Ga p_x orbitals from the first layer, and the second one consists of Ga p_z and s orbitals, with strong contributions from the underlying As p_z orbitals. Along $\overline{\Gamma J}$ and $\overline{\Gamma J'}$ the dangling bond state is in resonance with bulk states. The surface resonances (c) and (d) consist of contributions of gallium and arsenic p orbitals representing back bond states. Near the edge to the heteropolar gap, a surface state (e) can be found. It consists of Ga s orbitals from the topmost layer with a small admixture of As p_z orbitals and becomes a resonance in the $\overline{\Gamma J}$ direction. Below the heteropolar gap, another surface resonance is found (f), which consists of As s orbitals.

The surface bands are apparent as peaks in the density of states (DOS) which is calculated for a series of $k_{\parallel}$ points. Figure 3 shows the DOS for the $\bar{\Gamma}$ point, which is of main interest for an understanding of photoemission in normal emission. Figure 3(a) presents the layer-resolved density of states for the first six GaAs layers and a bulk layer, and Fig. 3(b) presents the orbital-resolved density of states for the first two atomic layers. The peaks, which belong to the sur-

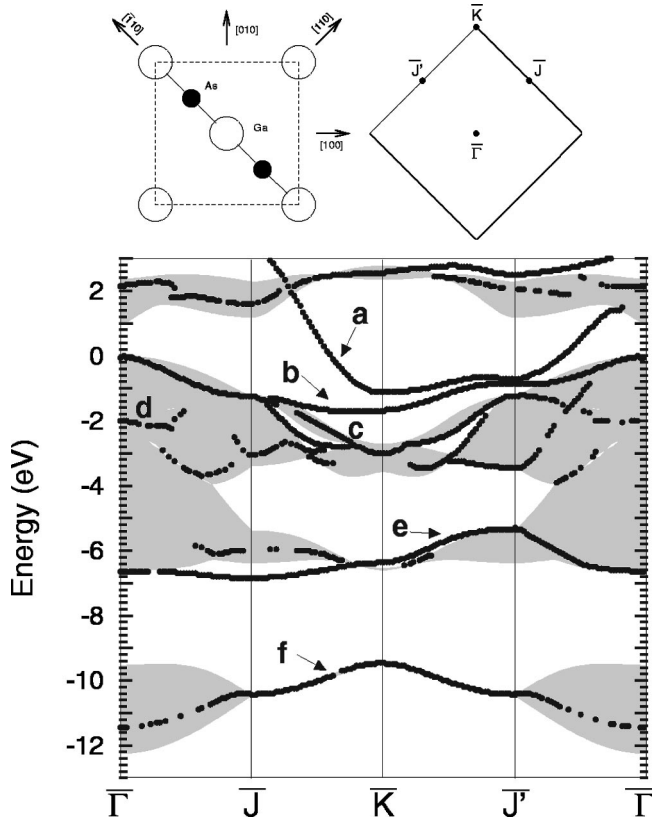

FIG. 2. Surface band structure of the GaAs(001)-(1×1)Ga surface and the projected bulk band structure of GaAs (shaded). The sketch shows the assumed ideal geometry of the GaAs(001)-(1×1)Ga surface (left side) and the surface Brillouin zone (right side). The gallium atoms of the first layer are presented by open circles, the arsenic atoms of the second layer by filled circles.

face bands (b), (d), and (e) (see Fig. 2) are clearly visible. Because of its vicinity to the band edge, the surface state (e) has a tail into the crystal.

Beside the initial states, in photoemission calculation, the final states are also needed. For the normal emission, Fig. 4 shows the complex-band structure of the GaAs(001) surface along $X-\Gamma-X$. The horizontal bars denote the weight with which individual complex bands contribute to the final state. Band (a) shows a dominant contribution to the final state and three other bands, marked by (b), (c), and (d), contribute much less.

Figure 5 shows the normal emission spectra from the GaAs(001)$-$(1×1)Ga surface, calculated for photon energies from 10 up to 45 eV. The light is incident in the [110] direction and is polarized parallel to the plane that is spanned by the [110] direction and the z axis. The polar angle of incidence is 45°. We find in the spectra several structures, which disperse with excitation energy [(B), (C), (D), (F), (G), and (H)]. Especially the structures (B) and (C) can be interpreted by assuming direct transitions. This means transitions between initial and final bands with exact conservation of the perpendicular component of the wave vector. For a given photon energy, the binding energies are determined at which transitions into the complex conduction-band structure are possible. These positions are indicated in the spectra by bars, whose lengths correlate with the contribution of the involved complex band to the final state. So the structures (B) and (C) can be connected with direct transitions from the initial state bands (1,2) and (3) (see Fig. 1) into the complex band (a) (see Fig. 4). The complex band (a) is the most important final band, which is consistent with the high intensity of these structures. It has to be pointed out that the structure (B) is not a purely bulk transition, since, especially for photon energies up to 24 eV, strong emissions from the broad maximum in the density of states of the first layer around -2.0 eV (see Fig. 3) contribute to this structure. As can be checked by the matrix elements for the chosen incident angles of the light, mainly the Ga and As p_x orbitals are responsible for these mixing. Beside the two main dispersing structures, there is one more dispersive peak (D) for photon energies between 14 and 27 eV. This weak structure is related to direct transitions from the initial band (1,2) to the final band (d). Furthermore, there are three other dispersive structures (F), (G), and (H), which are direct transitions to more weakly coupled final bands and, therefore, have only weak intensity.

In addition to the dispersive structures, the spectra show some nondispersive emissions. The state (A) can be seen for all excitation energies and results from emissions from the Ga and As p_z orbitals, located near the valence-band maximum, see Fig. 3. The matrix elements (see Fig. 6) emphasize that for photon energy less than 13 eV, the Ga p_z part dominates, while for higher photon energies, the As p_z part is the largest. Furthermore, for photon energies around 10 eV structure (A) is superimposed by direct emission from bulk bands near the valence-band maximum. The valence-band maximum itself is reached for a photon energy of 10.5 eV, which matches the crossing of final band (d) (see Fig. 4) with the Γ line. A second nondispersive structure in Fig. 5 is peak (E) at -6.6 eV. This structure is energetically in accordance with the strong Ga s and faint As p_z peak from the DOS in Fig. 3. The matrix elements from Fig. 6 and the strong peak in the DOS (Fig. 3) suggest that emissions from the Ga s orbitals dominate. This association is stressed by the fact that the peak maximum as a function of photon energy occurs at

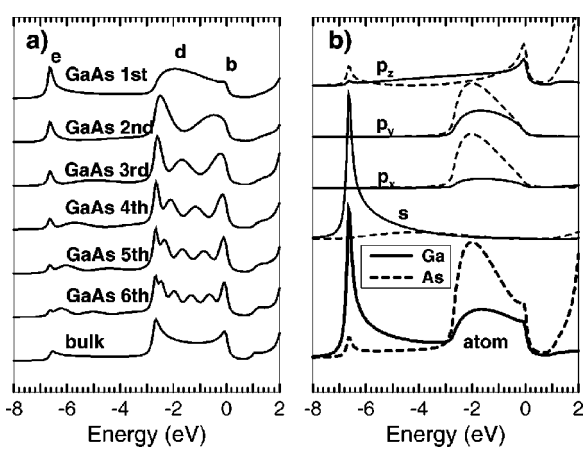

FIG. 3. Density of states for GaAs(001)-(1×1)Ga at the $\bar{\Gamma}$ point: the DOS resolved by layers (a) the DOS of the first GaAs layer resolved by atoms and orbitals (b).

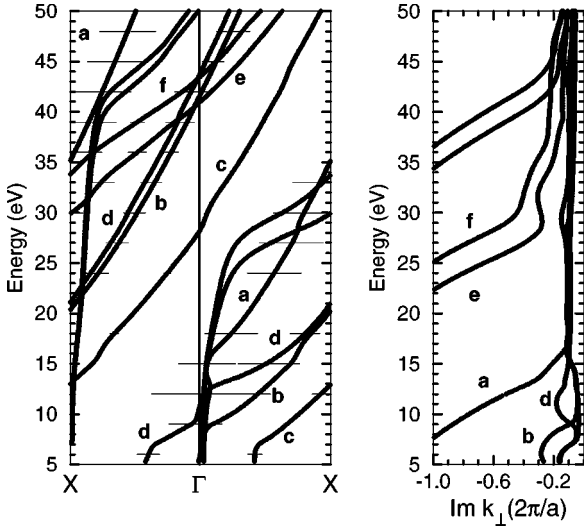

FIG. 4. Complex band structure of GaAs(001) for the symmetry line $\Delta = X\Gamma X$, from negative to positive $k_\perp$. There is no reflection symmetry because it describes only the propagation direction from crystal to vacuum. Bars indicate by their length the magnitude of the expansion coefficients of the final state with respect to the complex bulk bands. Right panel shows the imaginary part associated pointwise with the real $k_\perp$ band as indexed by letters.

19 eV in agreement with the maximum of the Ga *s* matrix element at about 12 eV final-state energy for a binding energy of 6.6 eV. Above 25 eV, the As p_z orbitals contribute, too. For photon energies above 38 eV, direct emissions from the valence band (3) (see Fig. 1) reach its lower band edge in this region and dominate the peaks.

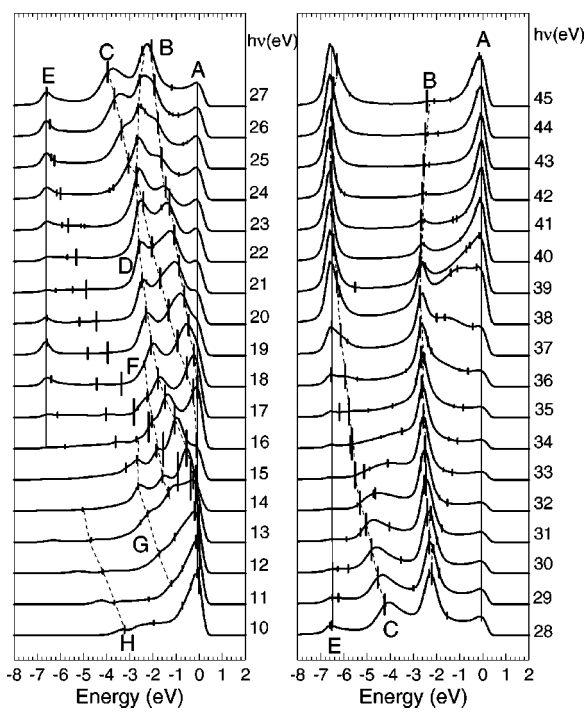

FIG. 5. Theoretical normal emission spectra for GaAs(001) $-(1\times1)$Ga. The bars indicate binding energies at which direct transitions would be expected. The lengths indicate the magnitude of the expansion coefficients of the final state.

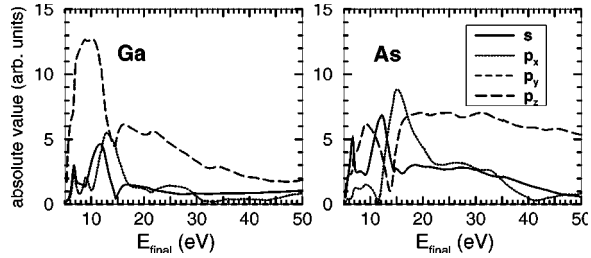

FIG. 6. Modulus of the matrix elements of the two outermost atomic layers of the GaAs(001)-(1×1)Ga surface resolved into orbitals.

The theoretical spectra in normal emission could be compared with experimental results. Olde *et al.*[15] and Cai *et al.*[16] present photoemission spectra in normal emission from GaAs(001)-$c(4\times4)$ and GaAs(001)-(1×1) surfaces, respectively. Both experimental data sets present strong dispersive structures, which can be associated with the strong emissions (*B*) and (*C*) in the theoretical spectra (see Fig. 5). Both experiments suggest emission from a surface state near the valence-band maximum (VBM), which can be explained by the emission (*A*) in Fig. 5. For photon energies lower than 30 eV, the variation in intensity of this peak is also correctly reproduced. Near the lower valence-band edge, both experiments show weak emissions, which agree with the emission from the surface state, marked by (*E*) in the theoretical spectra. The data from Cai *et al.*, measured up to 50.5 eV photon energy, show that for excitation energies above 38 eV, the emissions near the lower valence-band edge converge with the dispersive structure, which is associated with (*C*) in theory and that the intensity near the band edge increases strongly in that region.

The major difference between the experimental and theoretical results is that between 32 and 37 eV excitation energy, structure (*C*) in theory is much less intense than in experiment. A previous calculation[13] predicts this structure with higher intensities. That this is not seen in this paper can be traced back to the different pseudopotential (necessary here because of the heterostructure) used for the final states.

Beside the initial states, Zhang *et al.*[17] also investigate the conduction-band structure up to 20 eV for the GaAs(001) surface. There is satisfying agreement with our final state bands with respect to number of bands, approximate position, and dispersion, on one hand, and with respect to their influence on the photoemission intensities, on the other hand. The experimental conduction-band structure shows a strongly dispersive band between 4.0 and 11.0 eV that can be related to the complex final band (*c*) (see Fig. 4) and a second one extending up from 15.0 eV, which can be identified with the complex band (*a*) in our calculation. The latter one is responsible for a strong dispersing peak in both photocurrents, in the experimental spectra of Zhang and in this paper. Between the two bands, experimental data provide two more bands, which can be identified with the complex bands (*b*) and (*d*) in Fig. 4. As in the experimental data of Zhang *et al.*, the final band (*d*) is related to a dispersive structure (*D*) in Fig. 5.

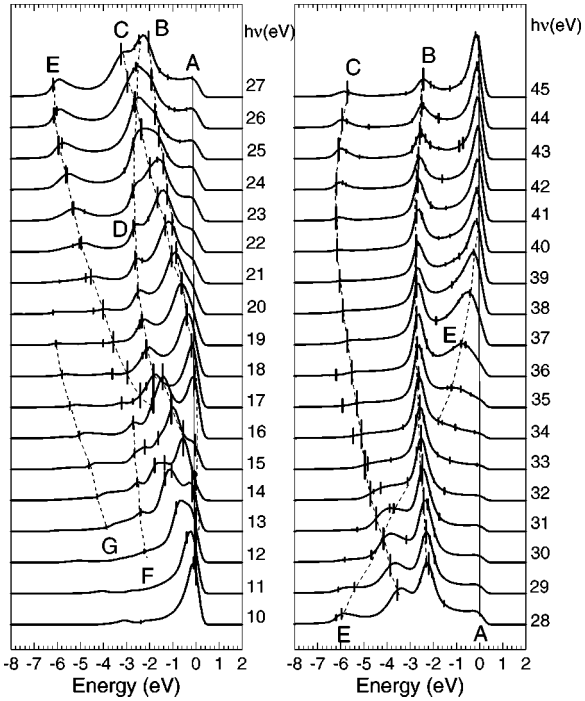

FIG. 7. Spectra in normal emission for AlAs(001)-(1×1)Al. For details see Fig. 5.

B. AlAs(001)-(1×1)Al

In this section our result for the AlAs(001)-(1×1)Al surface will be presented. The geometry is chosen as in the GaAs(001)-(1×1)Ga case (see Fig. 2), except that the Ga atoms are replaced by Al. The surface band structure looks very similar to the corresponding one of GaAs, as does the layer-resolved density of states. As in the GaAs case, the density of states at $\bar{\Gamma}$ shows a dangling bond state near the upper valence-band edge, which is caused by Al and As p_z orbitals. The back bonds near -2.0 eV correspond to their counterparts in the GaAs case. There is a difference between GaAs and AlAs regarding the cation p_z and anion s contributions, which are much wider in the AlAs case than for GaAs. Exceptionally, the counterpart to the Ga s surface state, which is located near the lower valence-band edge for GaAs [see Fig. 3(a), structure (e)] and exhibits strong resonance into the bulk, is missed in the AlAs case.

Figure 7 shows the spectra in normal emission for the AlAs(001)-(1×1)Al surface. The light is chosen as in the case of GaAs (see above). As for GaAs (see Fig. 5) the spectra show a nondispersive structure near the VBM. It is due to the DOS from the Al and As p_z states, which are located near 0.0 eV. An inspection of the matrix elements suggests that for photon energies less that 30 eV, the Al p_z orbitals dominate the photocurrent, while for higher excitation energies, the As p_z orbitals dominate. As expected from above the second nondispersive structure, which has been seen in the GaAs spectra near the lower valence-band edge (Fig. 5) is missed for AlAs. As for GaAs the AlAs spectra are dominated by two dispersive structures (B) and (C). They are caused by direct transitions from the initial band (1,2) and (3) (see Fig. 1) into the most important complex band for the final state. Beside these two structures, there are further, four dispersive structures (D), (E), (F), and (G), which can be related to transitions into complex bands, which contribute less to the final state. Especially, the dispersive structure (E) between 32 and 45 eV photon energy shows an interesting behavior. Despite its origin from direct transitions into weak final states, it dominates the photocurrent for high-excitation energies. For photon energies above 40 eV, it mixes with the emission from the surface state (A), resulting in a notably enhanced photocurrent.

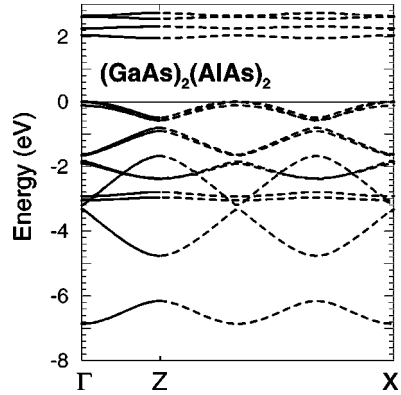

FIG. 8. Bulk band structure for the $(AlAs)_2(GaAs)_2$ superlattice. The real Brillouin zone terminates at Z; the bands are continued up to the X point.

C. $(AlAs)_2(GaAs)_2$(001)-(1×1)Ga

In this section, we present our results for a $(AlAs)_2(GaAs)_2$(001)-(1×1)Ga surface. The bulk crystal consists of pairs of GaAs bilayers, alternating with pairs of AlAs bilayers. The surface consists of two GaAs bilayers, whose geometry is analogous to that given in Fig. 2. Figure 8 shows the bulk band structure for the $(AlAs)_2(GaAs)_2$ superlattice in the ΓZ direction, relevant for normal photoemission from the (001) surface. For the superlattice, the symmetry of the Brillouin zone changes from face-centered cubic for GaAs and AlAs to a tetragonal one. The length between Γ and Z corresponds to one-quarter of the original ΓX distance. A first impression of the resulting band structure can be given by backfolding of the bulk valence bands into the smaller Brillouin zone, together with the opening of band gaps at their edges. For a better comparison with the GaAs and AlAs bulk crystals (see Fig. 1) the band structure is repeated up to the X point. A comparison between Fig. 1 and Fig. 8 shows that the band width of the whole set of valence bands above the heteropolar gap of the superlattice is comparable to that of bulk GaAs. Furthermore, we recognize the opening of the minigaps for the superlattice at the edge of the Brillouin zone near Z, particularly near -6.0 eV binding energy. The band structure can be compared to results from Gopalan *et al.*[12] In their calculation, the band structure shows a minigap near -6.0 eV, which has half the width of that in this paper. Furthermore, the results of Gopalan *et al.* include a band between -0.3 and -1.2 eV, which is more dispersive than its counterpart in this work. Apart from this, the two calculations show a reasonable agreement up to 7 eV

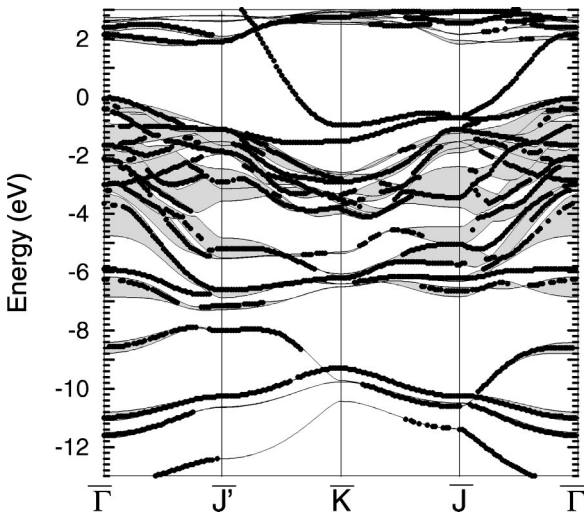

FIG. 9. Surface band structure for $(AlAs)_2(GaAs)_2(001)$-(1×1)Ga.

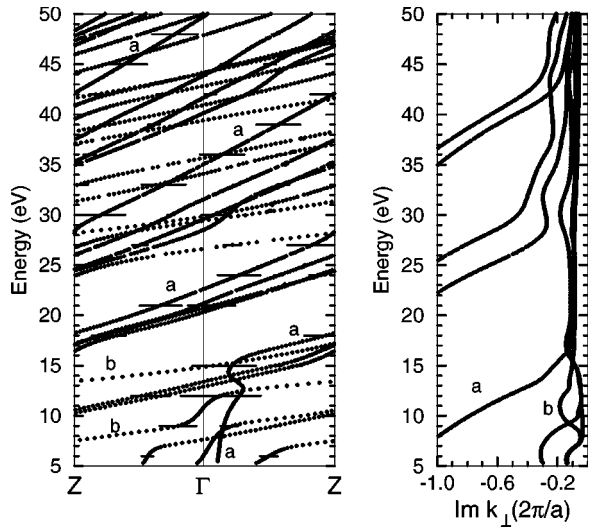

FIG. 10. Complex band structure of $(AlAs)_2(GaAs)_2(001)$. For details, see Fig. 4.

binding energy. Also, similar electron confinement of the valence-band top to the GaAs region is found in the calculations for the bulk, the surface region deviates slightly from the bulk in this respect, however.

The minigaps near the edge of the Brillouin zone are also responsible for the gaps in the projected bulk band structure for the $(AlAs)_2(GaAs)_2(001)$-(1×1)Ga surface (see Fig. 9). As for the GaAs(001)-(1×1)Ga surface (see Fig. 2) the most prominent surface states are the dangling and bridge bond states in the fundamental gap, whose orbital composition matches the GaAs(001)-(1×1)Ga case. For higher-binding energies there are some more surface bands for the superlattice than for the clean bulk crystal, which are mainly due to Ga and As p orbitals. Near -6 eV, we can find the analog to the surface state (e) from the GaAs(001)-(1×1)Ga surface (Fig. 2), i.e., a Ga s related surface state.

The smaller Brillouin zone in the z direction is also responsible for backfolding in the complex final bands (Fig. 10). As for the GaAs(001)-(1×1)Ga case (Fig. 4), there is one band that contributes most to the final state (a). Especially for higher energies, its dispersion fits the backfolded trend from the final band (a) in Fig. 4. Beside the final band (a) (Fig. 10) there is one more band (b), from which contributions to the photocurrent for lower-excitation energies could be expected.

Figure 11 shows the calculated photoemission spectra for the $(AlAs)_2(GaAs)_2(001)$-(1×1)Ga surface. The energy ranges and the direction of light are chosen as for the pure compounds above. Compared to GaAs(001)-(1×1)Ga (see Fig. 5) the spectra in Fig. 11 show much less dispersion in peak positions. The dispersionless Ga s and As p_z related structure (E) at -6.8 eV is shifted to -6.0 eV binding energy [structure (E) in Fig. 11]. This is the split-off state originating from the surface state that lies at -6.8 eV in the homogeneous GaAs and that is introduced by the superstructure because of its large penetration into the bulk. This case demonstrates that electron energy splittings in superlattices take place not only among delocalized states but also in not-too-strongly localized states. For lower-excitation energy, the peak (E) shows a similar intensity development as for the GaAs(001)-(1×1)Ga surface structure (E); this is striking but also obvious, if one compares the matrix elements that are very similar for both surfaces, see Fig. 6. The differences in intensity for excitation energies above 40 eV can be related to the band edge, which is reached in this energy region for GaAs(001). It should be taken into account that the surface emission (E) lies close to the lower border of the minigap generated by the superlattice. This fact should be taken into account in the identification of the minigap width from the experiment. Like GaAs(001)-(1×1)Ga surface, the $(AlAs)_2(GaAs)_2(001)$-(1×1)Ga shows a strong emission

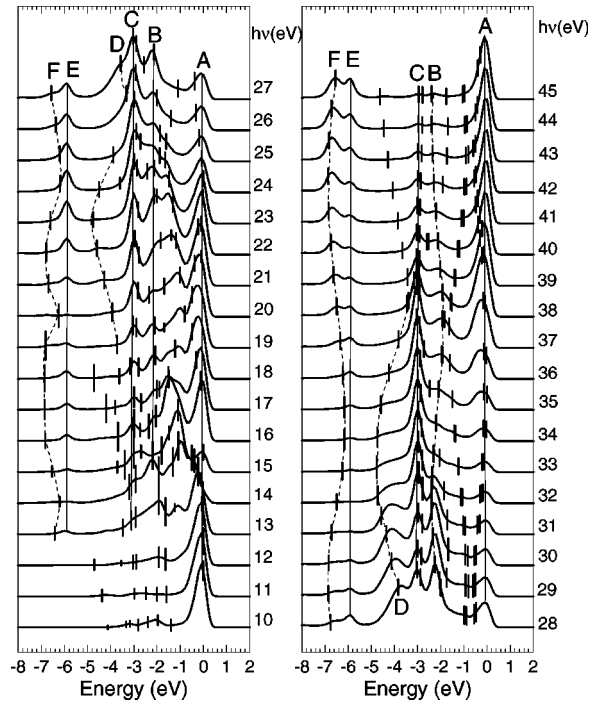

FIG. 11. Spectra in normal emission for $(AlAs)_2(GaAs)_2(001)$-(1×1)Ga. For details, see Fig. 5.

near 0.0 eV, which is more or less dispersionless and more intense than for GaAs(001). This emission is caused by Ga and As p_z surface orbitals like its counterpart in GaAs(100). For 11.0, 23.0, and 35.0 eV excitation energy, this emission is superimposed by direct transitions from the VBM into the final state band (a) (Fig. 10).

Near the lower valence-band edge at -6.9 eV there is a weakly dispersing structure (F), which is also caused by direct transitions into the final state (a). This structure becomes clearly visible for photon energies above 37 eV. At lower-binding energies, there is a second dispersive structure (D) between 26 and 38 eV photon energy. These two dispersive structures are kept apart by the minigap, formed at the Brillouin zone edge Z (Fig. 8) around -6.0 eV. In the case of GaAs(001)-(1×1)Ga (see Fig. 5) there is one single structure (C) that disperses continuously across this energy range to the lower valence-band edge. Therefore, the existence of the minigap in the photoemission spectra represents a pronounced characteristic property of the superlattice. Weak emissions from the upper border of the minigap are also visible for excitation energies between 19 and 25 eV in Fig. 11.

For lower-binding energies, the GaAs(001)-(1×1)Ga spectra show a dispersive emission (B) (see Fig. 5) which is caused by direct transitions and contains notable contributions from the surface. For $(AlAs)_2(GaAs)_2$(001)-(1×1)Ga there are two almost dispersionless structures nearby [(B) and (C), see Fig. 11]. The structure (C) is located near -3.0 eV. In this energy region, direct emissions from the nearly dispersionless bulk bands around -3.0 eV could be expected (Fig. 8). A more detailed evaluation shows that beside direct transitions, mainly emissions from the density of states contribute to the structure (C). In particular, emissions from the As p_x orbitals, located between the second GaAs and the first AlAs bilayer could be identified. The strongest evidence for this location is given by an inspection of the matrix elements (not shown). The matrix elements of the above mentioned As p_x orbitals decrease remarkably for final-state energies above 35 eV. This is consistent with the decreasing intensity of structure (C) for photon energies above 38 eV.

The second dispersionless structure (B) is located near -2.2 eV binding energy. Of course, this emission is influenced by different direct transitions, which cross this region. Especially for 18 and 19 eV photon energies, contributions from bulk emission can be found in the layer-resolved photocurrent, which will be discussed below. For photon energies between 21.0 and 25.0 eV, the main contribution is related to the third and fourth bilayers, which consist of AlAs. From the matrix elements and the DOS, we expect primarily emissions from the As p_x and the Al p_z orbitals in this energy region. For higher-photon energies (above 27 eV), the photocurrent has its source additionally in the first and second GaAs bilayer, where emissions from As and Ga p_x are expected. Figure 12 shows the layer-resolved photocurrent for three selected photon energies. Thick lines give total contribution of the two bilayers of GaAs or AlAs. At these energies we can identify the origin of the emission (B), i.e., originating from bulk emission, predominantly from the 3/4 AlAs bilayer, and predominantly from the topmost GaAs bilayer, respectively.

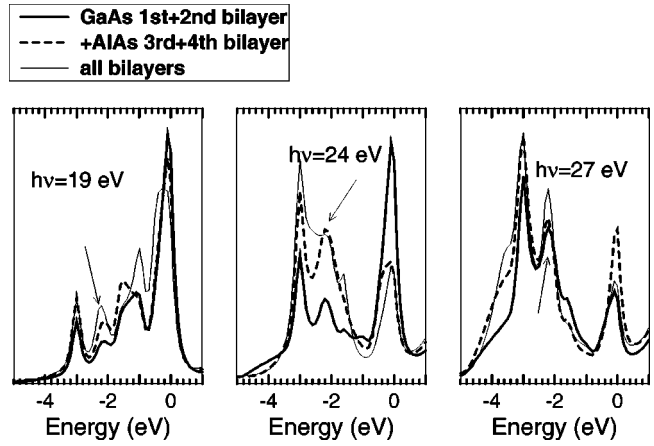

FIG. 12. Layer-resolved and layer-integrated photocurrent (normal emission) for $(AlAs)_2(GaAs)_2$(001)-(1×1)Ga, calculated for three different photon energies. The spectra are not broadened with an experimental resolution and were not multiplied by a Fermi distribution. Thick solid lines represent the photocurrent from the first two GaAs bilayers, while the thick dashed lines show the photocurrent integrated from the first two GaAs and AlAs bilayers. The thin lines illustrate the contribution of all 36 bilayers, taken into account in the calculation.

The theoretical data are compared to experiment. Cai *et al.*[18] published normal emission data from a (1×1) reconstructed (001) surface of a $(GaAs)_2(AlAs)_2$ superlattices. Their data are measured for photon energies from 24.80 up to 45.71 eV. The experimental spectra show much fewer structures than does our theory (Fig. 11); in addition, the experimental spectra are crossed by second- and third-order emission from As $3d$ and Al $2p$ core lines. Clearly visible is a structure with less dispersion near the lower valence-band edge, which can be attributed to the emission (E) and (F) in Fig. 11. Between 24.80 and 31.73 eV photon energy, Cai *et al.* observe a dispersive structure, which agrees with the structure (D) in Fig. 11. The main difference is that in this paper the structure (D) is visible for a photon energy above 27 eV, while it is seen in experiment for the few measured lower-excitation energies as well. Furthermore, the theoretical spectra possess strong emissions between -1.0 and -3.0 eV binding energy. These emissions are missed in experiment. As the most important result, the calculated spectra confirm the experimentally observed band-gap opening near the lower valence band edge. Detailed discussion will require better resolved experimental data.

D. $(AlAs)_3(GaAs)_3$(001)-(1×1)Ga

In this section, the results for $(AlAs)_3(GaAs)_3$(001)-(1×1)Ga are presented and discussed. As seen in Fig. 13, the addition of one more layer of GaAs and of AlAs into the superlattice unit cell, gives rise to an additional minigap near -3.4 eV, while the bandwidth for the whole set of valence

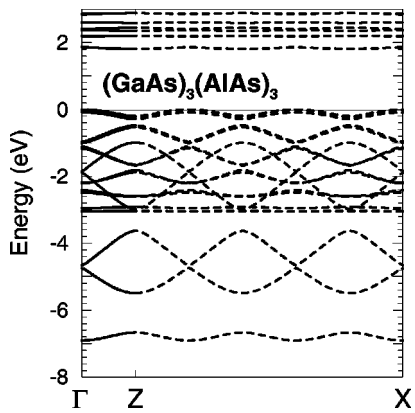

FIG. 13. Bulk band structure for the $(AlAs)_3(GaAs)_3$ superlattice.

bands above the heteropolar gap of 6.91 eV remains nearly unchanged compared to Fig. 8. This main new feature fits into the trend of electron band-structure transformation with the thickness of superlattice components given by diminishing size of the Brillouin zone (perpendicular to the surface). In particular, in the lower half of the valence band, related to the light-hole branch of the electron dispersion of GaAs, this effect is clear, undisturbed by mixture with the heavy-hole derived branches. The new band gap is also visible in the projected bulk band structure (see Fig. 14) and is accompanied by a surface state near its upper edge at $\bar{\Gamma}$ and $\bar{K}$. The Ga *s* surface state, which was discussed in the last section is now shifted to higher binding energy (compared to Fig. 9) and lies in the middle of the minigap around -6.2 eV. Compared to the $(AlAs)_2(GaAs)_2(001)$-(1×1)Ga surface, $(AlAs)_3(GaAs)_3(001)$-(1×1)Ga shows many more surface states and resonances.

In Fig. 15 the calculated photoemission spectra in normal emission are shown. As in the case of $(AlAs)_2(GaAs)_2(001)$-(1×1)Ga (see Fig. 11) in the spectra two nondispersive structures are found. One is located at

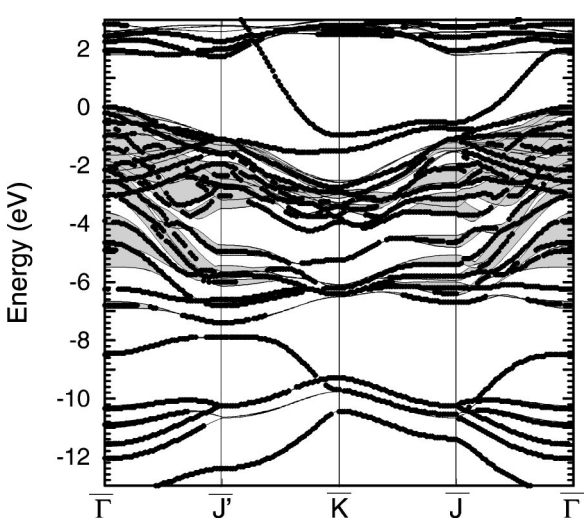

FIG. 14. Surface band structure for $(AlAs)_3(GaAs)_3(001)$-(1×1)Ga.

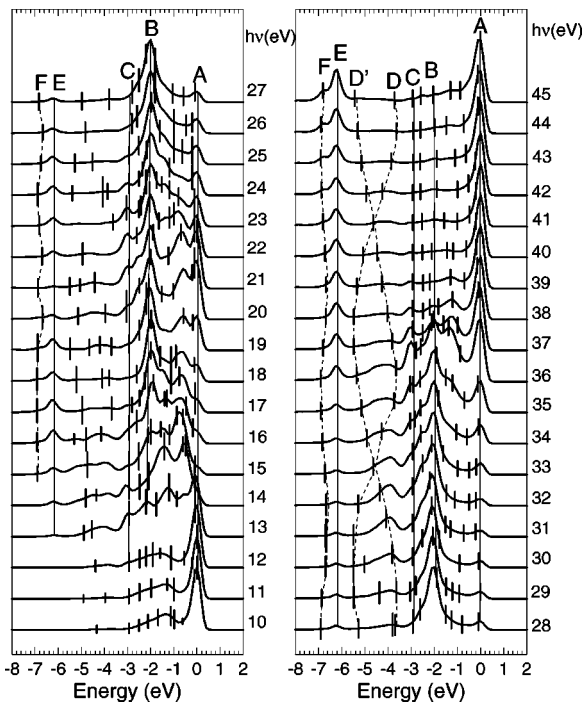

FIG. 15. Spectra in normal emission for $(AlAs)_3(GaAs)_3(001)$-(1×1)Ga. For details, see Fig. 5.

-6.0 eV and belongs to the Ga *s* and As p_z related surface state [structure (E)] in the minigap around -6.0 eV. As could be verified by the matrix elements, the orbital composition of this peak is mainly Ga *s* derived. The second one (A) is located near 0 eV binding energy and consists of emissions from the Ga and As p_z orbitals. Both maxima from (A) at 10 and 21 eV photon energy are related to maxima in the Ga p_z matrix elements (not shown), while for higher-excitation energies the As p_z elements dominate.

Below structure (E) small shoulders (F) become visible for excitation energies about 43.0 eV, which belong to direct transitions from the lower valence-band edge. For photon energies near 39 eV, this emission marks the lower boundary of the minigap, which opens around -6.0 eV (see Fig. 13). At -3.4 eV, all the spectra show a minimum in intensity. This minimum belongs to the second opened minigap in Fig. 13 around -3.4 eV. Between both gaps, there are two dispersive structures visible in the spectra [(D) and (D')], which are caused by direct transitions from the bulk bands between the two gaps. Above -3.4 eV, we find two dispersionless structures (B) and (C). For structure (C) at -3.0 eV, we find emissions from the AlAs layers below the first three GaAs layers, which was determined from the layer-resolved photocurrent (not shown). The orbital composition of this peak is related to Al and As p_x orbitals. Although there should be emission from direct transitions, because there are two nearly dispersionless bulk bands at -3.0 eV (Fig. 13), this possibility is only visible around 13.0 eV photon energy, as could be verified by the layer-resolved photocurrent. Another dispersionless structure (B) is found at -2.0 eV. This emission is mainly affected by the

first three GaAs layers. Based on the matrix elements and the DOS, these emissions come from Ga and As p_x orbitals.

Summarizing, the $(AlAs)_3(GaAs)_3(001)$-(1×1)Ga system shows an additional minigap at around -3.4 eV. Emissions from the AlAs bilayer buried below three GaAs layers can still be detected.

IV. CONCLUSION

The theoretical investigation of very thin superlattices shows that angle-resolved normal emission photoelectron spectroscopy can detect the period of the lattice according to specific minigaps in the electron-band structure. The effect is pronounced and within the scope of actual experimental resolution, as was confirmed by a former experiment on a 2×2-lattice. Despite the close similarity of GaAs and AlAs spectra, which has its origin in similar bandstructures of both uniform systems, the compound structure of the superlattice does not display simply an average of the spectra of its constituents. Thus, the differences in the potential between both materials are strong enough to generate a new system.

First, the photoemission peak dispersion over a wide range of excitation energies, i.e., several tens of eV, is broken into several segments in superlattices leaving only a few regions where dispersion can be observed. This dispersive structure can be seen qualitatively to repeat in the sequence of spectra, parametrized by the photon energy as a consequence of the superlattice's backfolding. Especially, the spectra of $(AlAs)_2(GaAs)_2$ show the required periodicity. For $(AlAs)_3(GaAs)_3$ with its minor dispersion, it would be difficult to determine the superlattice's periodicity only from the periodicity of the spectra with respect to their dependence on photon energy. The curvature of the bulk band structure is lost in the spectra. It results from the finite peak widths, the dispersionless surface and interface states, and the minigaps compressing, and thus, flattening the band structure in the remaining binding-energy interval. Three clearly visible structures are seen in the 2×2 superlattice, which preserve the strong dispersion of both constituents. The dispersion of the other maxima is either absent (localized surface states) or weak because of the above-mentioned flattening.

Second, the opening of the minigap between -5.0 and -6.0 eV is obvious though a surface state is observed at the lower gap edge for normal emission. Both constituents GaAs and AlAs show emissions within this gap, therefore, this gap alone is sufficient to identify the superlattice behavior. In the 3×3 case, the minigaps are harder to be identified from the spectra because clear dispersive peaks close to the band edges are absent.

Third, the surface state of one constituent (GaAs), at -6.7 eV in the homogeneous system, is split because of its extent into the bulk that is affected by the superlattice. It consists of one at the same energetic position with similar orbital composition, namely Ga s orbitals, and of one moved into the new gap opening in the band above the original state. The latter contains additional Ga p_z and As p_z orbitals. As can be demonstrated by a simple one-dimensional example, this state corresponds to an ''antibonding'' configuration of adjacent orbitals in the enlarged supercell, whereas the former state reflects the original bonding situation in this cell. The above holds for all three superlattices (1×1) (not shown here), (2×2) and (3×3).

All three properties can be independently used to identify a superlattice system from measured spectra of the constituents and the composite alone. The results suggest that tailoring the valence bands with desired properties is feasible also on a nanoscale and may be successfully controlled by photoemission. The detailed analysis of the origin of emissions reveals that excitations even from below the third layer are accessible and clearly distinguishable by photoemission. However, it should have become obvious that accurate numerical one-step calculations are required for a successful interpretation of such experimental data.

ACKNOWLEDGMENTS

The work was supported by the DAAD and the BMBF, under Contract Nos. 05 SB8 FKA7 and TSR-075-97, as well as by NSF Contract No. INT-9815358. It was supported in part by the Director, Office of Science, Basic Energy Sciences, Materials Sciences Division, of the U.S. Department of Energy under Contract No. DE-AC03-76SF00098.

[1] E.E. Mendez and K. von Klitzing, *Physics and Application of Quantum Wells and Superlattices* (Plenum, New York, 1987).

[2] M.J. Kelly, *Low Dimensional Semiconductors: Materials, Physics, Technology, Devices* (Clarendon, Oxford, 1995).

[3] D.J. Arent, R. Alonso, G. Horner, M. Bode, J.M. Olson, X. Yin, M.C. DeLong, A.J. SpringThorpe, and A. Majeed, J. Vac. Sci. Technol. B **12**, 1009 (1994).

[4] T. Strasser, C. Solterbeck, W. Schattke, I. Bartoš, M. Cukr, and P. Jiříček, Phys. Rev. B **63**, 085309 (2001).

[5] J. Henk, W. Schattke, H.P. Barnscheidt, C. Janowitz, R. Manzke, and M. Skibowski, Phys. Rev. B **39**, 13 286 (1989).

[6] J. Henk, W. Schattke, H. Carstensen, R. Manzke, and M. Skibowski, Phys. Rev. B **47**, 2251 (1993).

[7] E. Clementi and C. Roetti, At. Data Nucl. Data Tables **14**, 177 (1974).

[8] R. Hoffmann, J. Chem. Phys. **39**, 1397 (1963).

[9] M. Wolfsberg and L. Helmholz, J. Chem. Phys. **20**, 837 (1952).

[10] F. Starrost, S. Bornholdt, C. Solterbeck, and W. Schattke, Phys. Rev. B **53**, 12 549 (1996); **54**, 17 226 (1996).

[11] E.T. Yu, D.H. Chow, and T.C. McGill, Phys. Rev. B **38**, 12 764 (1988).

[12] S. Gopalan, N.E. Christensen, and M. Cardona, Phys. Rev. B **39**, 5165 (1989).

[13] T. Strasser, F. Starrost, C. Solterbeck, and W. Schattke, Phys. Rev. B **56**, 13 326 (1997).

[14] K.A. Mäder and A. Zunger, Phys. Rev. B **50**, 17 393 (1994).

[15] J. Olde, G. Mante, H.-P. Barnscheidt, L. Kipp, J.-C. Kuhr, R. Manzke, M. Skibowski, J. Henk, and W. Schattke, Phys. Rev. B **41**, 9958 (1990).
[16] Y.Q. Cai, A.P.J. Stampfl, J.D. Riley, R.C.G. Leckey, B. Usher, and L. Ley, Phys. Rev. B **46**, 6891 (1992).
[17] X.D. Zhang, J.D. Riley, R.C.G. Leckey, and L. Ley, Phys. Rev. B **48**, 17 077 (1993).
[18] Y.Q. Cai, J.D. Riley, R.C.G. Leckey, B. Usher, J. Fraxedas, and L. Ley, Phys. Rev. B **44**, 3787 (1991).